# ACOUSTICAL PROPERTIES OF RANDOMLY ROUGH SURFACES

**P Boulanger** **The University of Hull, Department of Engineering, Hull HU6 7RX**
**K Attenborough** **The University of Hull, Department of Engineering, Hull HU6 7RX**

## 1. INTRODUCTION

The objective of this work is to develop models that will evaluate impedance spectra for various rough-hard surfaces corresponding to different sea states. The main effect of surface impedance on sonic boom propagation is in the shadow zone. Less important effects are also in the primary carpet, where the incidence angle varies quite significantly. This work is focused on grazing angle which is the propagation angle of the series of creeping waves diffracting into the shadow zone. The specific impedance of sea water is greater than that of air by four orders of magnitude, therefore the sea surface is considered to be acoustically hard for atmospheric sound propagation. The roughness will be considered static and the effect of the diffraction of sound waves by roughness is modelled as an effective admittance although, in reality, the scattered field is not constant because the boundary is continously in movement due to winds and currents.

## 2. THE ACOUSTIC MODELS

### 2.1. The Boundary Element Model (BEM)

The method used in this work was developed by Chandler-Wilde[i],[ii] who solved the Helmholtz equation for the pressure at the receiver with the boundary integral equation:

$$P(\vec{r},\vec{r}_0) = G_\beta(\vec{r}_0,\vec{r}) + \int_\gamma \left\{ \frac{\partial G_\beta(\vec{r}_s,\vec{r})}{\partial n(\vec{r}_s)} - ik\beta(\vec{r}_s) G_\beta(\vec{r}_s,\vec{r}) \right\} P(\vec{r}_s,\vec{r}_0) ds(\vec{r}_s) \tag{1}$$

where $P(\vec{r},\vec{r}_0)$ is the pressure at the point $\vec{r}$ when the source is at $\vec{r}_0$. The integral extends over the ground surface $\gamma$ which is either the part of the surface impedance $\beta$ lying above the horizontal or the part of the boundary with a normalized surface admittance $\beta(\vec{r}_s)$. $G_\beta(\vec{r}_0,\vec{r})$ is the Green function for the Helmholtz equation in a half plane with impedance boundary condition and can be calculated analytically. The boundary integral equation is solved approximately by assuming a constant pressure value in each boundary element of the ground surface. A flat or profiled ground surface can be modelled as the discretizing points can be chosen out of the horizontal plane. Source, receiver and specular point are assumed to be in a vertical plane perpendicular to the roughness axis, and a line integral is solved. The BEM is applied to predict sound levels over rough surfaces by including the roughness profile under the form of node coordinates input to the program. In order to model the rough surface correctly, it is necessary to use boundary element lengths that are smaller than the smallest segment between two nodes. A second constraint for an accurate use of the boundary element technique is the need to choose boundary element lengths no more than one fifth of the wave-length. The first and second constraints govern computation times at low frequencies and high frequencies respectively. In all cases modelled in this work, the hard surfaces are modelled with an admittance $\beta$=0.

The BEM proved to be an accurate model when compared to results from past experiments involving mixed impedance[iii] and rough ground[iv]. The BEM is considered in this work as the reference to which the Twersky theory is compared.

### 2.2. Twersky's Theory

Twersky has developed a boss model[v],[vi],[vii],[viii] to describe coherent reflection from a hard surface containing semi-cylindrical roughnesses in which the contributions of the scatterers are summed to obtained the total scattered field. Sparse and closely-packed distributions of bosses have been considered and interaction between neighbouring scatterers has been included. His results lead to a real part of the effective admittance of the rough hard surface which may be attributed to incoherent scattering. The effective relative admittance $\beta$ of a rough hard surface containing non-periodically-spaced 2-D circular semi-cylinders is expressed as:

$$\beta = \eta - i\xi, \tag{2}$$

where

$$\xi(\alpha,\varphi) \approx kV\left[-1+\left(\delta\cos^2(\varphi)+\sin^2(\varphi)\right)\sin^2(\alpha)\right]+O(k^3) \tag{3}$$

and

$$\eta(\alpha,\varphi) \approx \frac{nk^3\pi^2a^4}{8}(1-W)^2\left\{\left(1-\sin^2\alpha\sin^2\varphi\right)\left[1+\left(\frac{\delta^2}{2}\cos^2\varphi-\sin^2\varphi\right)\sin^2\alpha\right]\right\}+O(k^5) \tag{4}$$

In these expressions, $V=n\pi a^2/2$ is the raised cross sectional area per unit length, $n$ is the number of semi-cylinders per unit length ($n$= 1/$b$), $\delta$ is a measure of the dipole coupling between the semi-cylinders, $(1-W)^2$ is a packing factor introduced for random distributions, $W = nb^* = \frac{b^*}{b}$, where $b$ is the average (center to center) separation between two cylinders, $b^*$ is the minimum separation between two cylinders, $a$ is the semi-cylinder radius and $k$ is the wave number. The angle of incidence with respect to the normal is named $\alpha$ and the azimuthal angle between the wave vector and the roughness axes $\varphi$. Twersky's effective admittance model is subject to the approximation $ka \le 1$.

## 3. EXCESS ATTENUATION AND BEM EFFECTIVE IMPEDANCE

### 3.1. Computation Method for Excess Attenuation

The excess attenuation wich is the attenuation of the sound wave in excess of that from spherical spreading is computed from both models by:

$$EA = 20\log\left|\frac{P}{P_1}\right| \tag{5}$$

where the direct wave is

$$P_1 = P_0\frac{\exp(ikR_1)}{R_1} \tag{6}$$

and where

$$P = P_0\frac{\exp(ikR_1)}{R_1} + QP_0\frac{\exp(ikR_2)}{R_2}. \tag{7}$$

The total pressure $P$ for the BEM and the model based on Twersky's theory are computed from equations (1) and (7) respectively and the distance $R_1$ and $R_2$ are shown in Figure 1. The model based on Twersky's theory incorporates the Weyl van der Pol spherical wave reflection coefficient Q.

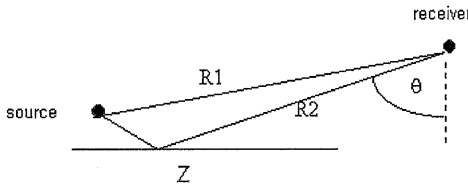


**Figure 1: Geometry used in the Weyl van der Pol formulation**

### 3.2. Effective Impedance from BEM Excess Attenuation

#### 3.2.1. The Admittance Root Equation

The excess attenuation (EA) computed with the BEM from equations (1), (5) and (6) corresponds to the attenuation due to the interference between the direct wave, the rough surface reflected wave and a possible surface wave. The method used to estimate the effective impedance of such a rough surface is to consider that this EA predicted by the BEM is produced by a flat surface of effective admittance $\beta_{ef}$ given by solving for the admittance in the Weyl van der Pol spherical wave reflection coefficient. The problem becomes a $\beta_{ef}$ root search for the following equation (8)

$$1+\frac{R_1}{R_2}e^{ik(R_1-R_2)}\left\{\frac{\cos\theta-\beta}{\cos\theta+\beta}+\left(1-\frac{\cos\theta-\beta}{\cos\theta+\beta}\right)\left(1+i\sqrt{\pi}\sqrt{ikR_2}/2\left(\beta+\cos\right.\right.\right.$$

where $F(w)$ is the sphericity factor. $w$ is often called the "numerical distance", and represents the propagation distance scaled by the impedance. This equation to be solved for each frequency point does not have a readily available analytical solution, therefore, numerical methods have to be sought. Two widely used numerical methods for root finding of complex variable equations have been implemented in this work. The Newton Raphson method that produces only one root per frequency point may be one of the most popular in the literature and has been reported[ix] previously in effective impedance estimations. The second method is based on an IMSL library routine based on Müller's technique that is limited practically to a couple roots for each frequency point. The weakness of these two methods is their potential lack of convergence toward a root for some frequency points, and the fact that they find at the best a couple roots. The lack of convergence was an obstacle on several test cases, but an important factor in this work was the need to insure that no physically meaningfull root was missed in the search. Therefore, a third more thorough root search method based on winding number integral has been developed.

#### 3.2.2. The Winding Number Integral Method

This root search method is based on the winding number integral which is a contour integral around a closed path in the complex plane to determine the presence of zeros and poles in the enclosed area. Having determined that a closed area in the complex plane contains roots, the location of those roots can be deduced with a high degree of accuracy by using higher moments of the winding integral. This method is described by Brazier–Smith et al.[x] who apply it to the determination of roots from dispersion equations. A summary of the method implemented in this work is presented next.

Let's assume that the roots of an function F, analytic everywhere inside a closed contour $\Gamma$, are sought, the difference between the number of zeros $n_Z$ and the number of poles $n_P$ of F inside $\Gamma$ can be computed from the winding integral.

$$\frac{1}{2\pi i}\oint_\Gamma \frac{F'}{F}dz = n_z - n_p \tag{9}$$

where the complex integral can be evaluated by the winding number of F($\Gamma$) around the origin in an anticlockwise path. The winding number is noted by $n_Z - n_P$ = Wnd(F($\Gamma$),0). Once the image of the closed contour $\Gamma$ is computed by the function F the path can be divided into a series of chords and each cord is tested to check if it takes Ln(F) across the negative real axis. If it crosses from above, the winding number is increased by one and if from below, reduced by 1one. When the number of zeros inside a contour is established, the roots need to be identified. This study considers the search of roots two at a time in a contour, therefore only the first two moments of the winding integral are required. The expression of a moment $I_n$ of order n is given by:

$$I_n = -\frac{1}{2\pi i}\left\{\left[z^n \ln F\right] - n\oint_\Gamma z^{n-1}\ln F dz\right\} = \sum_i \left(z_z^i\right)^n - \sum_j \left(z_p^j\right)^n \tag{10}$$

where $z_z^i$ is the location of the $i^{th}$ zero and where $z_p^j$ is the location of the $j^{th}$ pole. Equation ) shows only one pole for $\beta = -\cos(\theta)$ therefore the expressions for the moments are simplified and contain only $z_z^i$ in most of the complex plane. When the winding number is equal to one, the single zero is given by $I_1$ and when the winding number is equal to 2, the two zeros are determined by the roots of the quadratic equation

$$z^2 - I_1 z + 0.5(I_1^2 - I_2) = 0 \tag{11}$$

Let's note that if three roots at a time were sought, the third moment of the winding number integral would be needed and the cubic equation given in Reference x would be used with correction of a typo. Indeed, the constant term in equation (9) of Reference x contains a factor incorrectly defined as $-(I_1^2)/6$ that should really be $-(I_1^3)/6$.
The integral shown in equation (11) is computed numerically with a Rieman sum. Great care has to be exercised when computing the function Ln($F$) because Ln is not analytical across the negative real axis and the argument $F$ of Ln might cross this branch cut. This potential discontinuity problem with Ln($F(z)$) is solved using an analytical continuation of Ln across the branch cut. Mathematically, this means that instead of considering Ln as a simple function, it is viewed as a familly of Ln functions each defined on a separate Riemanian sheet. This allows the continuity of the Ln($F(z)$) family function at each branch cut, a branch cut being viewed as a seem of two successive Riemannian sheets. Practically, this means that instead of considering Ln($F$) as the function with argument $\theta$ only such that $-\pi<\theta<\pi$ (as Fortran does) and getting a discontinuity when $\theta$ increases beyond $\pi$, one requires the argument of Ln to increase by $2\pi$. Therefore, when $\text{Arg}(F(z))=\theta$ increases n times beyond $\pi$, $\text{Arg}(F(z))=\theta + 2n\pi$ , and one uses

$$\text{Ln}(F(Z)) = \text{Ln}|F(z)| + i\text{Arg}\{F(z)\} + 2n\pi i \qquad (12)$$

When applied to the admittance root equation ), the method uses a series of square contours $\Gamma$ in which the roots are searched. If more than 2 roots are detected with the winding number count inside each square contour $\Gamma$, a smaller contour is chosen.

## 4 EXPERIMENTS

The experimental results have been described in detail in other work[iv] and a brief summary is presented. A Tannoy driver, fitted with a 1m long tube having 3 cm internal diameter was used as a point source. The receiver was a Bruel & Kjaer type 4311 "half-inch" diameter condenser microphone fitted with a preamplifier. Signal processing and signal generation were carried out using a maximum length sequence system analyzer. To calculate the Excess Attenuation, a reference measurement was made with source and receiver at the maximum height of 2m allowed by the suspending cable above the floor of the anechoic chamber. Varnished halves of 1 m long, large and small radius wooden dowel rods were taped on to the boards to act as cylindrical two-dimensional roughness. The smaller rods have semi-elliptical cross sections with major axis (base) of 0.0135 m and semi-minor axis (height) of 0.005 m. The larger rods are more semicircular in cross section and have been modelled as perfectly semicircular with radius 0.02 m. The point source and receiver were suspended 0.1m above the board surface and 1 m apart. Random distributions were studied for both types of rods using, in turn, 20 small semi-cylindrical rods, 12 large semi-cylindrical rods. The positions of the rods were determined by using random number tables.

## 5. EXCESS ATTENUATION AND EFFECTIVE IMPEDANCE RESULTS FOR RANDOM DISTRIBUTIONS OF SEMI-CYLINDERS AND PARABOLIC ROUGHNESS

In the following, d is the source-receiver separation distance, h is the source and receiver heights, $h_{eff}$ is the effective source and receiver height when a non nominal value is used, l=2a is the semi-cylinder diameter, w is the length of ground modelled in the BEM and Z is the impedance.

### 4.1 Small Hard Randomly Spaced Semi-Cylinders

#### 4.1.1 Excess Attenuation Results

The measurements and BEM predictions used a 20 hard semi-cylinder roughness profile with l=0.0135m, d=1m and h=0.1m. The following compares the BEM EA (dashed line) with measured data (solid line) and Twersky's theory (dotted line) using $h_{eff}$= 0.111m, l=0.08m and the other parameters with nominal values. These parameters have been varied to match the BEM and measured results. The best agreement with the BEM is obtained when using an effective source and receiver height $h_{eff}$ =0.111m higher than the nominal 0.1m. The dotted-dashed line is obtained from the effective impedance computed from measured Excess Attenuation. The results are very close to the measurements up to 8000Hz and show that the effective impedance presented next allows to reproduce measured excess attenuation for a wide range of frequencies.

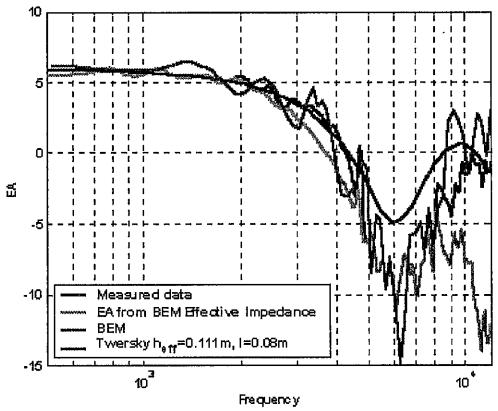


**Figure 2: Excess attenuation above a small semi- cylindrical roughness profile**

#### 4.1.2 Effective Impedance

The following effective impedance is computed from the measured EA with a ground plane effective height set to the top of the random roughness ($h_{ef}$=0.093m), and any negative Re(Z) set to zero. The method of raised effective impedance plane has been reported before[xi],[xii] and allows, in this work, to obtain real effective impedances with physically meaningfull values. This method is applied systematically in all effective admittance calculations reported in this work from measurements or BEM predictions. The curves on the top and bottom half of the graph show respectively, the real part and the negative of the imaginary part of the effective impedance.

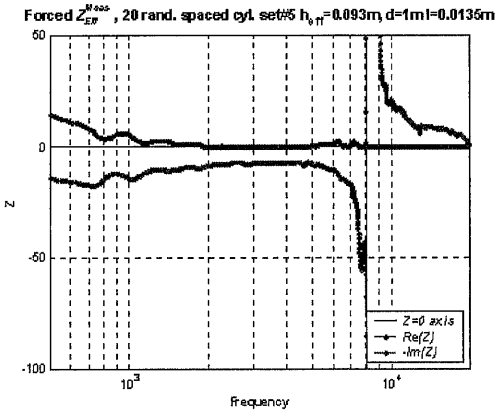


**Figure 3: Effective impedance computed from measured data for a small semi- cylindrical roughness profile**

The following effective impedance is computed from the BEM EA. The curves on top and bottom half of the graph show, respectively, the real part and the negative of the imaginary part of the effective impedance.

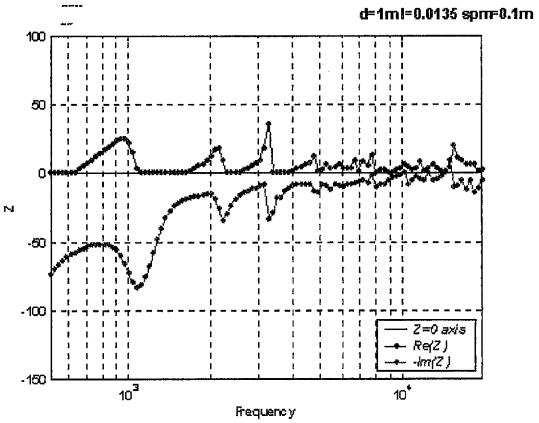


**Figure 4: Effective impedance computed from BEM data for a small semi- cylindrical roughness profile**

The Excess Attenuation obtained from the above BEM effective impedance are quasi identical to the Excess Attenuation predicted by the BEM from the nominal source and receiver heights and are not presented.

The effective impedance from Twersky's theory is presented next.

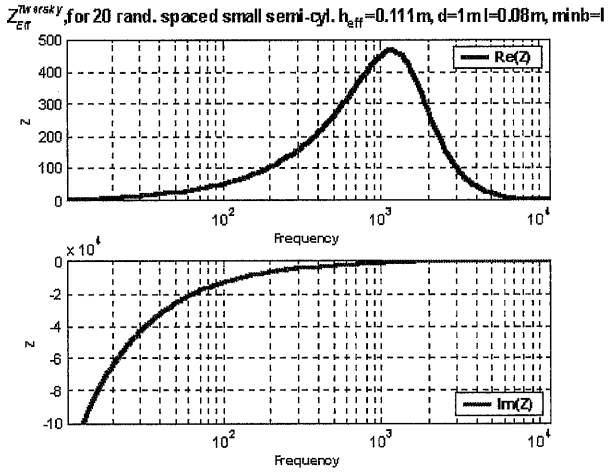


**Figure 5: Effective impedance computed from Twersky's theory for a small semi- cylindrical roughness profile**

## 4.2 Larger Randomly Spaced semi-Cylinders

### 4.2.1 Excess Attenuation Results

The measurements and BEM predictions used a twelve hard semi-cylinder roughness profile with l=0.04m, d=1m and h=0.1m. The following graph compares the BEM EA (dashed line) with measured data (solid line) and Twersky's theory (dotted line). Twersky's model used an effective source height $h_{eff}$= 0.17m and a semi-cylinder diameter l=0.13m. The minimum center to center separation distance in Twersky's model is chosen to be

equal to the semi-cylinder diameter (b*=l) although b*= 0.047m in the BEM, and all other parameters have nominal values. The parameters in Twersky's model have been varied to improve the agreement with the BEM results.

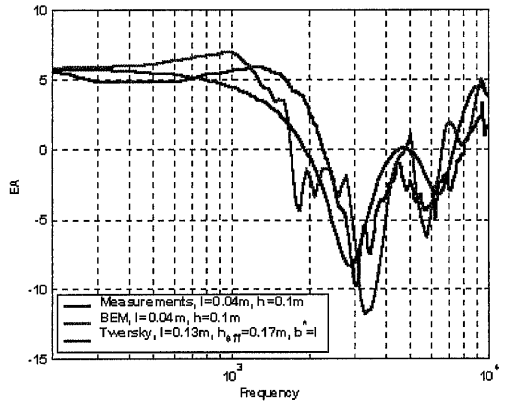


**Figure 6: Excess attenuation above a large semi- cylindrical roughness profile**

### 4.2.2 Effective Impedance

The following effective impedance is computed from the BEM Excess Attenuation. The curves on top and bottom half of the graph show respectively, the real part and the negative of the imaginary part of the effective impedance.

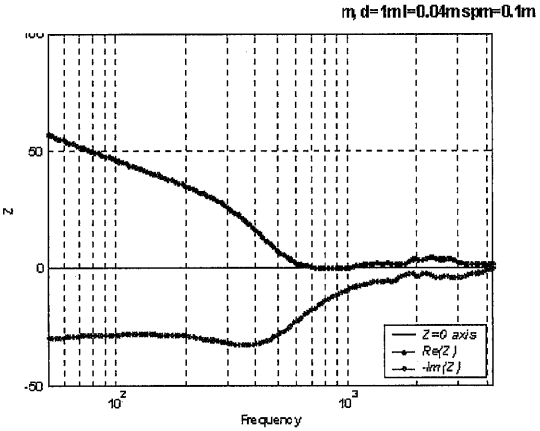


**Figure 7: Effective impedance computed from BEM data for a large semi-cylindrical roughness profile**

The EA curve obtained from the above BEM effective impedance is identical to the nominal BEM EA and is not presented. This is expected as only one data point real part around 700Hz is forced to zero.

The effective impedance from measured data is shown next. The curves on top and bottom half of the graph show, respectively, the real part and the negative of the imaginary part of the effective impedance. The real part is forced to zero only for frequencies above 10000Hz and the excess attenuation will then be identical to the measurements below 10000Hz.

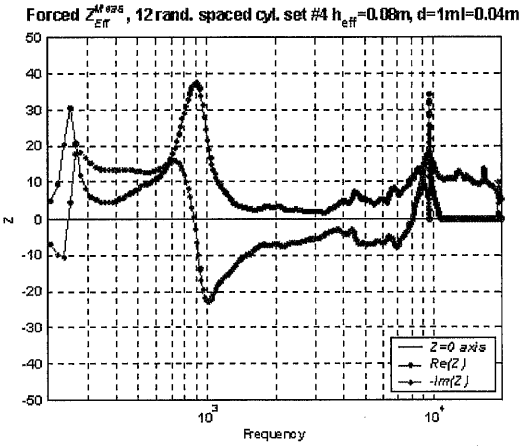


**Figure 8: Effective impedance computed from measured data for a large semi-cylindrical roughness profile**

The effective impedance from Twersky's theory is presented next.

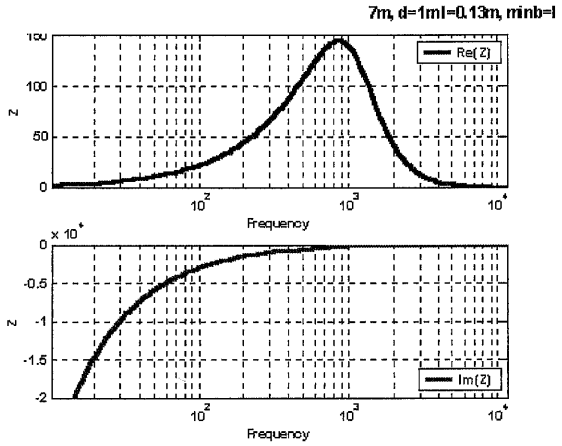


**Figure 9: Twersky's theory Effective impedance for a large semi-cylindrical roughness profile**

### 4.3 Large Parabolically Shaped Random Roughness

In order to model a more realistic water wave roughness profile, parabolic shapes are investigated. The geometry for this case corresponds to a source and receiver height of h=0.93m, and a separation source-receiver d=8m. No measurements are available and only model results are reported. The BEM is used with (a) a small length (2m) of rough ground beyond the source and receiver and (b) with an additional 9m of flat hard surface on each side as seen partially below. The roughness heights Hm are randomly generated in the range [0.1m-0.4m] and the relation Hm/L=0.14 is used to evaluate the wave-length L of the parabolic roughness.

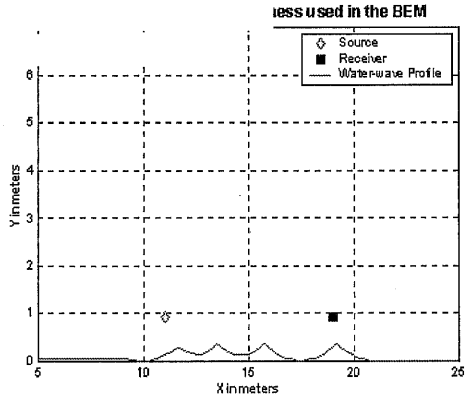


**Figure 10: Large random parabolic roughness profile**

#### 4.3.1 Excess Attenuation Results

The following graph compares the BEM EA results for case (a) (dotted dashed line) and (b) (dashed line) with Twersky's theory (dotted line) that used seven semi-cylinders with diameter l=0.3m and effective height $h_{ef}$=1.1m. These parameters are varied to match the BEM results and the best agreement is obtained when using a source and receiver height greater than the nominal 0.93m of the BEM. The solid line shows the EA results when using the BEM effective impedance obtained below. The nominal BEM results are reproduced fairly well below 2500Hz. Significant differences in BEM EA spectra are obtained from the additional flat ground modelled on both sides of the source and receiver (case (b)). This effect will have to be considered when trying to model longer portions of roughness profiles where cpu-time limitations will impose restrictions on the ground length modelled.

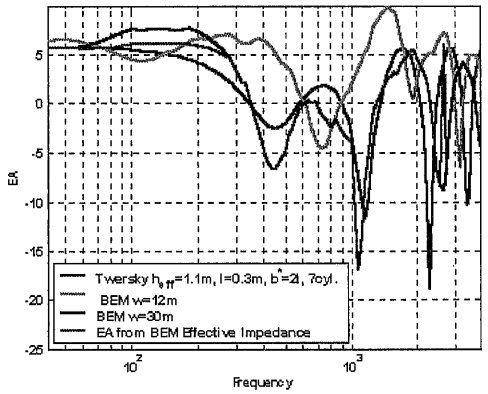


**Figure 11: Excess attenuation above a large parabolic random roughness profile**

#### 4.3.2 Effective Impedance Results

The following results show the effective impedance obtained from the BEM data assuming that the effective impedance plane is 0.2m above the trough of the lowest roughness (0.15m below the maximum roughness height) and setting to zero any negative Re(Z). The curve entirely in the positive half of the plane shows the real part of the effective impedance.

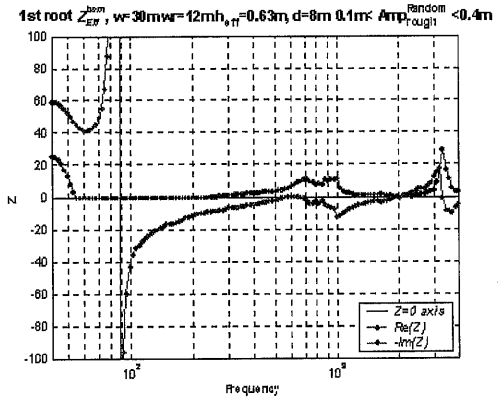


**Figure 12: Effective impedance computed from BEM data for a large parabolic random roughness profile**

The effective impedance obtained from Twersky's theory is shown next

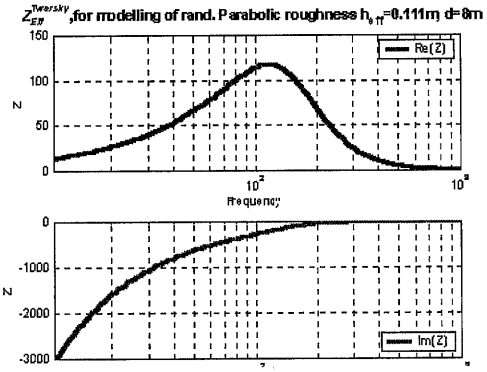


**Figure 13: Twersky's theory effective impedance**

## 4. CONCLUSIONS

Two methods have been developed to model the acoustical properties of random hard rough surfaces. One is based on the effective impedance evaluated from solving the impedance roots from the Weyl van der Pol expression based on the complex excess attenuation predicted by a Boundary Element Method. The effective impedance can be used in a Weyl van der Pol expression that models a flat ground to reproduce the predicted BEM excess attenuation. The second method is an analytical technique based on a boss theory from Twersky where the contributions from semi-cylindrical or elliptical rough scatterers are summed to obtained the total scattered field. This theory evaluates the effective impedance from coherent reflection and incoherent scattering from a rough hard surface leading respectively to the imaginary and real part of the effective impedance. Semi-cylindrical and parabolic randomly spaced roughness profiles have been modelled and some results have been compared with experiments. A satisfactory agreement is found for Excess Attenuation results but different effective impedance spectra are obtained which generate these attenuation curves. This will be subject to further investigation. It is found for measured data and BEM simulations that the effective impedance plane has to be raised to obtain physically meaningfull values of effective impedance real part. In order to obtain satisfactory agreement between Twerky's theory and BEM or measured results, it is found also that the effective impedance plane in Twersky's model has to be lowered and the size of the semi-cylinders increased.

[i] Chandler-Wilde S. N. and Hothersall D. C. "Efficient calculation of the green function for acoustic propagation above a homogeneous impedance plane ", J. Sound and Vib., **180**, 705-724 (1995).

[ii] Chandler-Wilde S. N. and Hothersall D. C., "A uniformly valid far field asymptotic expansion of the green function for two-dimensional propagation above a homogeneous impedance plane" ", J. Sound and Vib., **182**, 665-675 (1995)

[iii] Boulanger P., Attenborough K. "Models and Measurements of Sound Propagation from a Point Source over Mixed Impedance Ground". J. Acoust. Soc. Am. **102**, 1432-1442 (1997).

[iv] Boulanger P, Attenborough K., Taherzadeh S., Waters-Fuller T., and Li K. M.,
Ground Effect Over Hard Rough Surfaces

[v] V. Twersky, "Scattering and reflection by elliptically striated surfaces" J. Acoust. Soc. Am. **40**, 883-895 (1966).

[vi] V. Twersky, "Multiple scattering of sound by correlated monolayers" J. Acoust. Soc. Am. **73**, 68-84 (1983).

[vii] V. Twersky, "Reflection and scattering of sound by correlated rough surfaces" J. Acoust. Soc. Am. **73**, 85-94 (1983).

[viii] R. J. Lucas and V. Twersky, "Coherent response to a point source irradiating a rough plane" J. Acoust. Soc. Am. **76**, 1847-1863 (1984).

[ix] Taherzadeh S. and Attenborough K., "Deduction of ground impedance from measurements of excess attenuation spectra" " J. Acoust. Soc. Am. **105**, 2039-2042 (1999).

[x] Brazier –Smith P. R. and Scott J. F. M., "On the determination of the roots of dispersion equations by use of winding number integrals", J. Sound Vib. **145**, 503-510 (1991).

[xi] Chambers J. P., Sabatier J. M. and Raspet R., "Grazing Incidence propagation over a soft rough surface", J. Acoust. Soc. Am. **102**, 55-59 (1997).

[xii] Allard J.F., Kelders L. and Lauriks W., "Ultrasonic surface waves above a doubly periodic grating", J. Acoust. Soc. Am. **105**, 2528-2531 (1999).